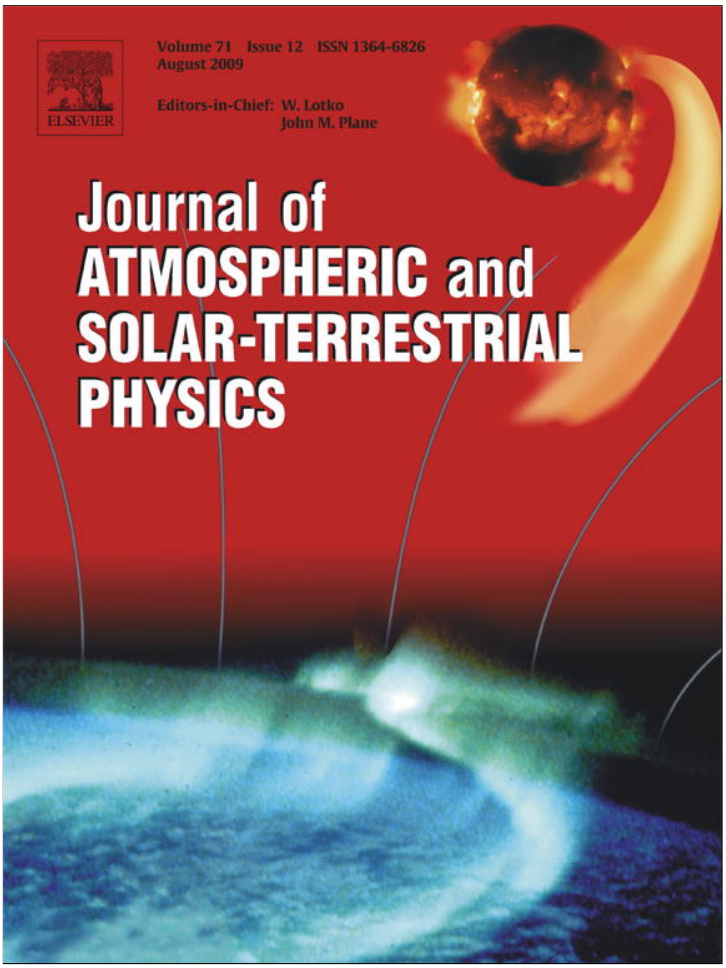

Journal of Atmospheric and Solar-Terrestrial Physics 71 (2009) 1322–1332

Contents lists available at ScienceDirect

Journal of Atmospheric and Solar-Terrestrial Physics

journal homepage: www.elsevier.com/locate/jastp

# Solar flare effect on the geomagnetic field and ionosphere

A. Meza [a,b,*], M.A. Van Zele [b,c], M. Rovira [b,d]

[a] Facultad de Cs. Astronómicas y Geofísicas, Universidad Nacional de La Plata, La Plata, Argentina
[b] Consejo Nacional de Investigaciones Científicas y Técnicas (CONICET), Buenos Aires, Argentina
[c] Facultad de Ciencias Exactas y Naturales, Universidad de Buenos Aires, Argentina
[d] Instituto de Astronomía y Física del Espacio (IAFE), Buenos Aires, Argentina

ARTICLE INFO

*Article history:*
Received 14 December 2007
Received in revised form
2 May 2009
Accepted 13 May 2009
Available online 7 June 2009

*Keywords:*
Solar flare effect
TEC
Geomagnetic field
GPS

ABSTRACT

This paper studies the ionospheric and geomagnetic response to an X6.2 solar flare recorded at 14:30 UT on December 13, 2001, in quiet geomagnetic conditions which allow the variations in the geomagnetic field and ionosphere measurements to be easily related to the solar flare radiation.

By using measurements from the global positioning system (GPS) and geomagnetic observatories, the temporal evolution of ionospheric total electron content variation, $vTEC_V$, and geomagnetic field variations, $\delta B$, as well as their rates of variation, were obtained around the subsolar point at different solar zenith angles. The enhancement of both parameters was recorded one to three minutes later than the Geostationary Operational Environmental Satellite (GOES) programme recording; such delay tends to depend on the latitude, longitude, and solar zenith angle of the observatory's observations.

The $vTEC_V$ is related to the local time and the $\delta B$ to the intensity and position of the ionospheric currents.

The $vTEC_V$'s maximum value is always recorded later than the maximum values reached by $\delta B$ and the X-ray intensity. The maximum $\delta B$ is larger in the local morning than in the afternoon.

The rates of $vTEC_V$ and $\delta B$ have two maximum values at the same time as the maximum values recorded by Hα (for each ribbon).

This work shows the quantitative and qualitative relations between a solar flare and the ionospheric and geomagnetic variations that it produces.



## 1. Introduction

Solar flares are one of the most powerful manifestations of the solar activity. Together with coronal mass ejections, the eruptive prominences and the solar wind are the solar events which affect the Earth's atmosphere. They were discovered in 1859 by Hodgson and Carrington independently when they were looking at the sunspot evolution. The energy is released as emitted radiation, accelerated particles, and bulk mass motion.

The different spectral ranges of the emitted radiation show a typical scheme. There is a "preflare" brightening generally lasting a few minutes, followed by the "impulsive" phase, which typically lasts a few minutes and consists of bursts in gamma rays, hard rays, EUV, and microwave radiation. After the impulsive phase, thermal radiation dominates; this is the gradual or decaying phase of the flare that can take several hours. The individual spikes have time scales of seconds or less. The evolution of soft X-rays is more similar to the Hα flare, without an impulsive phase. Because of their morphology, flares are divided into two types. One is the so-called compact flare, a brightening of coronal radiations. The second is the two-ribbon flare, which in Hα has its flash phase marked by the brightening of two narrow ribbons, one to each side of a neutral line. The flare in this analysis belongs to the last type.

The ionospheric solar flare effect (isfe) is analysed from the variation in the vertical total electron content (*vTEC*) data obtained from GPS. The isfe affects the *vTEC* behaviour, causing a sudden increase in total electron content (SITEC), whose intensity depends on the solar flare intensity and localisation (Liu et al., 2006) and on the location of the GPS station. SITEC has been investigated by several authors since the 1970s (Thome and Wagner, 1971; Mendillo et al., 1974; Davies, 1980); their researches were based on the measurements of operating VHF radio beacons on geostationary satellites and on incoherent scatter observations. The increase in electron density during solar flare occurs in every region of the ionosphere but the increase in electron density in the F region is thought to be responsible for a large fraction of the SITEC (Mendillo, 1974).

The main problems of the existing methods of studying isfe are the discontinuous, non-global monitoring of sudden ionospheric disturbances and inadequate space–time resolution. At present,

* Corresponding author at: Facultad de Cs. Astronómicas y Geofísicas, Universidad Nacional de La Plata, La Plata, Argentina.
*E-mail address:* ameza@fcaglp.fcaglp.unlp.edu.ar (A. Meza).

1364-6826/$ - see front matter © 2009 Elsevier Ltd. All rights reserved.
doi:10.1016/j.jastp.2009.05.015

the global positioning system (GPS), which is a powerful and mature geodesic tool, is widely used for a broad range of technological and scientific applications. The observation of permanent GPS tracking stations, under the management of the International GPS Service (IGS), has become a powerful tool for ionospheric research, providing good, continuous worldwide coverage at low cost to the users. Many authors have used GPS for total electron content (TEC) observations and in the study of ionospheric space weather (Aarons et al., 1997; Ho et al., 1998; Jakowski et al., 1999; Afraimovich et al., 2000; Meza et al., 2005), especially for SITEC properties (Afraimovich, 2001, 2002, 2000; Zhang et al., 2002; Zhang and Xiao, 2003, 2005; Liu et al., 2004, 2006; Wan et al., 2005; García Rigo et al., 2007). In particular, Zhang et al. (2002) analysed the ionospheric response to a solar flare similar to the flare used in this work; they found that the enhancement of TEC tended to depend on latitude, longitude, and the solar zenith angle of the subionospheric point, but not symmetrically, and it was smaller in the local morning than in the afternoon. The work of Zhang et al. (2002) was carried out during perturbed geomagnetic days. Donnelly (1976) found that the amplitude of the ionospheric response decreased with the angular distance of the flare from the central meridian of the Sun. Zhang and Xiao (2000) and Matsoukas et al. (1972) studied the ionospheric response of the region at different local times. Zhang and Xiao (2000) concluded that the response to the flare in the region occurring in the local morning is stronger than in the afternoon, this result being quite different from those obtained by Matsoukas et al. (1972) and Zhang et al. (2002).

The geomagnetic solar flare effect (gsfe) is the magnetic increase in the geomagnetic field of the whole dayside hemisphere of the Earth; it is detected as a field fluctuation with a rapid rise to maximum intensity, then a slow steady decline. It was called a "crochet" in the early works.

Because the far UV and soft and hard X-ray solar flare radiation (1–1000 Å) is absorbed by the ionosphere, the ionisation density increases unevenly at different heights, enhancing the ionospheric conductivity in the lower ionosphere (D and E regions). The currents that produce the gsfe depend on the thermal and tidal air movement, the magnetic field of the Earth at ionospheric heights, and the distribution of the conductivity (Van Sabben, 1961), forming an independent current system of the Sq (Volland and Taubenheim, 1958). The gsfe is the result of a temporary enhancement of solar ionising radiation without any change in the electric field (Rastogi, 1998); therefore, it is significantly affected by the extra electron production due to the intensity of solar flare radiation. The gsfe is sometimes difficult to identify among other phenomena like those produced by Earth's currents, sudden storm commencements, substorms, and neutral winds, because their geomagnetic variations are similar.

Although there are many authors who have worked on the gsfe phenomenon, reference will be made to some researches that have proved to be very useful for our analysis. Lui et al. (1996) found that during a solar flare, only the intensity of the solar radiation determined the magnitude of the geomagnetic field strength, the amplitude of gsfe was related to the local time in a similar way to the Sq current, and the maximum value was determined around local noon for different latitudes. Van Sabben (1961) showed that the ionospheric northern current vortex that generates the gsfe is generally centered to the west of the southern current vortex and is generally at a higher latitude than the Sq current. Curto et al. (1994) studied the gsfe at Ebro observatory, located near the focus latitude; they found reversed current especially in the hours before local noon and at equinox, which proved that the currents that produced the gsfe were not a simple increase in the Sq diurnal variation. Nagata (1952) showed that the gsfe at Huancayo (dip 1°N) under the equatorial electrojet (centered around the dip equator) is abnormally large. The enhancement of the Sq daily variation over the magnetic equator was associated with abnormal electrical conductivities due to the cross magnetic and electric fields in the E region, where the mobility of the ions and electrons is different (Baker and Martyn, 1953). Rastogi et al. (1965) showed that during gsfe the enhancement of the H field amplitude in the equatorial American zone is more pronounced than in the Indian zone when similar variations in the strength of the electrojet current are recorded in both regions.

The aim of this work is to analyze the effect of a flare on the ionosphere and the geomagnetic field. To obtain reliable conclusions, we analyze a flare developed during a quiet geomagnetic interval.

## 2. Observations

The flare which took place on December 13, 2001, a geomagnetic quiet day, was a 3B flare (in Hα classification) reported by RAMEY (Ramey Air Base, Puerto Rico). It started at 14:24 UT, attained its maximum intensity at 14:30 UT, and ended at around 15:45 UT. It was located at N16 E09 in the National Oceanic and Atmospheric Administration (NOAA) 9733 region. The region was classified as UF, meaning that it has many eruptive centers and two bright regions that identify the "two-ribbon" flares (in morphological classification). It was also observed by GOES.

To analyse the response of the global ionosphere to the extra radiation emitted by this solar flare, we compute *vTEC*. The *vTEC* measurements are obtained from the observables of a ground-based GPS receiver that belongs to IGS. To this end, the code-delay ionospheric observable is modeled using an arc-dependent bias, $\tilde{b}_{arc}$, in the equation of observation (Ciraolo et al., 2007), instead of a classical receiver-dependent bias (Sardon et al., 1994).

The ionosphere is approximated by a single shell of infinitesimal thickness with equivalent TEC, located 450 km above the Earth's surface. An obliquity factor equal to $1/\cos z'$ is used to map *vTEC* into *sTEC*, $z'$ being the zenithal distance of the slant path at the piercing point of the signal on the shell, which is the point where the signal crosses the ionospheric shell, and

$$sTEC = \frac{1}{\cos z'} vTEC.$$

Daily solutions are computed to estimate the arc-dependent bias, $\tilde{b}_{arc}$, using the GPS observations of the station. To reduce errors due to the obliquity factor, only observations with $z' < 25^\circ$ were considered.

To analyse isfe from *vTEC* obtained from GPS data, we work with one, two, or sometimes three *vTEC* curves that belong to different satellites.

The parameters used in this analysis are: the amplitude of the *vTEC* variation with respect to a quiet condition ($vTEC_V$) and the rate of this variation ($rvTEC$) (Afraimovich et al., 2000; Wan et al., 2005).

The variation in *v*TEC, $vTEC_V$, is defined by

$$vTEC_V(t_k) = vTEC(t_k) - vTEC_M(t_k), \tag{2.1}$$

where $vTEC_M$ is the value that *vTEC* achieves in quiet conditions (without isfe) and $t_k$ is the time.

The *vTEC* variation rate, $rvTEC_V$, is defined by

$$rvTEC_V(t_{k+1}) = \frac{vTEC_V(t_{k+1}) - vTEC_V(t_k)}{\Delta t_k}, \tag{2.2}$$

where $\Delta t_k = t_{k+1} - t_k$.

To study the geomagnetic field variation produced by the solar flare effect (sfe), we use the geomagnetic field, $\vec{B}$ $(X, Y, Z)$ recorded every minute by geomagnetic field observatories (freely available from Kyoto WDC). The difference between $\vec{B}$ affected by sfe and $\vec{B}$ in quiet conditions is defined by $\overrightarrow{\delta B}$. $\vec{B}$ in quiet conditions is represented for each component by a straight line defined by two points: one recorded in the last quiet moments (before the gsfe is detected) and the other reached immediately after the gsfe has disappeared.

Therefore, the amplitude of the gsfe is calculated as

$$\delta B = ((\delta X)^2 + (\delta Y)^2 + (\delta Z)^2)^{1/2} \tag{2.3}$$

The $\delta B$ variation, $(\delta B)'$, is defined by

$$(\delta B)' = \frac{\delta B_i - \delta B_{i-1}}{\delta t} \tag{2.4}$$

where $\delta t = 1$ min.

In this work, the isfe is detected from the *vTEC* variation, $vTEC_v$, where the electron contents from the lower to the higher part of the ionosphere are considered; then *vTECv* takes into account both the ionisation of the lower ionosphere by hard X-rays (from 2 to 260 Å) and in particular that of the upper ionosphere by soft X-rays or EUV, while the gsfe, measured by the $\delta B$, is the consequence of currents in the lower ionosphere.

## 3. Results

### 3.1. Solar flare measurements

For December 13, 2001, the GOES which observes in an energy range between 1 and 8 Å gives the following information: a flare starts at 14:20 UT, reaches it maximum at 14:30 UT, and ends at 14:35 UT according to the *Solar Geophysical Data*, where the data are reported every 5 min. The reported coordinates are N16 E09 and the X classification is X6.2 (intensity $6.2 \times 10^{-1}$ erg cm$^{-2}$ s$^{-1}$).

If a graph of the GOES intensity is made as a function of the time with a point every minute (from the National Geophysical Data Center), it can be seen that the intensity begins to increase from 14:23 UT (the last quiet value) (see Fig. 1).

For the Hα telescope for Argentina (HASTA), the intensity begins to increase at the same time, about 14:24 UT, and the maximum is recorded between 14:28 and 14:29 UT, 1 min before the RAMEY station report.

In Fig. 2, the intensity of each ribbon (Hα wavelength) recorded by HASTA every 20 s is shown. The curve on the left shows two maxima, the first at approximately 14:26 UT and the second between 14:28 and 14:29 UT, while the one on the right shows only one maximum between 14:28 and 14:30 UT.

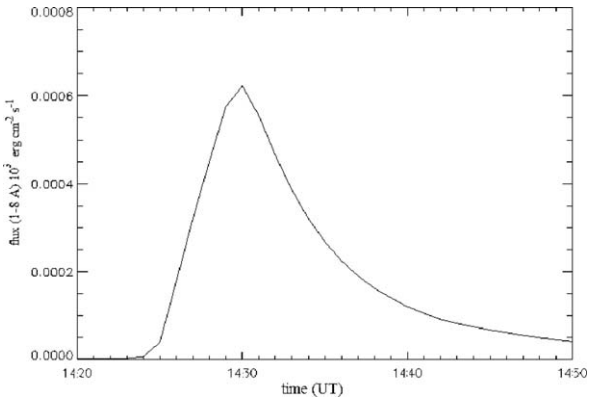


**Fig. 1.** X-ray flux (1–8 Å) recorded by GOES each minute on December 13, 2001, during a solar flare; here, 14:23 UT is considered to be the last quiet minute before the flare; the maximum is recorded at 14:30 UT.

### 3.2. vTEC measurements

After careful selection, the *vTECs* computed (Meza et al., 2005) from 41 GPS stations are analysed. Table 1 shows the names of GPS receivers, listed from lower to higher solar zenith distance, their geographic coordinates, the maximum value of $vTEC_v$, max $vTEC_V$ (Eq. (2.1)), the last quiet time before the isfe is detected, and, whenever possible, the time when the maximum value is recorded.

Table 1 shows that the isfe starts at different times depending on the solar zenith distance; the larger the solar zenith angle, the later the beginning of the isfe. The beginning of the isfe is one to two minutes after the flare is recorded by GOES satellite (14:23 UT, see Section 2). The largest maximum $vTEC_v$ is 6 TECU and is also correlated with the solar zenith angle; the smaller the solar zenith angle, the larger the maximum $vTEC_v$ value, which is also correlated with the solar zenith distance.

Fig. 3 shows the daily *vTEC* obtained from the previous method at ALGO GPS station on December 13, 2001. Systematic differences in the *vTEC* obtained at the same instant by different satellites can be observed in Fig. 3 because of their different positions during their paths inside the circle of 25° of radius around the zenith of the station. The *vTEC* values obtained from a satellite to the south of the receiving station are higher than those computed from a satellite to the north of the receiving station which is located in the Northern Hemisphere; the opposite would be the case if the station were located in the Southern Hemisphere.

Figs. 4 and 5 show the $vTEC_V$ (Eq. (2.1)) and $rvTEC_V$ (Eq. (2.2)) for one satellite using ALGO GPS station observations. Both figures show that the last quiet time isfe value is at 14:25 UT, because the amplitude of the variation at this time is larger than the previous ones and the last quiet time in *rvTEC* is represented by the last value near zero. Fig. 5 shows two large intensifications, the first at 14:26 UT and the second at 14:29 UT.

Fig. 6 shows that although the isfe depends on the solar zenith distance, the stations located to its northwest (in the local morning) have larger values of $vTEC_V$ than those located to its northeast (in the local afternoon).

Fig. 7 shows the geographic distribution of the max $vTEC_V$. Table 2 shows the maximum values of $rvTEC_V$ (Eq. (2.2)) (in TECU/min) and the times when they happen; when the solar zenith angle is lower than 79°, the value of the first maximum is always larger than the second one and in the rest of the cases both maxima have similar values or the second one is the largest.

From the previous $vTEC_V(t_k)$ and $rvTEC_V(t_k)$ results, we can point out the following general characteristics:

- The beginning of isfe is recorded between 14:24 and 14:25 UT and its maximum value between 14:30.5 and 14:35.5 UT. The earliest times of isfe commencement and its maximum value are recorded by GPS stations located close to SSP.
- There are two maxima of $rvTEC_V(t_{k+1})$: the first is at 14:26.5 UT and the second at 14:29 UT. The value of the first maximum is in general larger than the second one. The larger values are recorded by GPS stations located close to SSP.

The amplitude of $vTEC_V(t_k)$ is related to the local time. The values are larger when the flare effect is recorded in the local morning rather than in the local afternoon.

### 3.3. Geomagnetic measurements

In Table 3, the geomagnetic observatories where the maximum of $\delta B$ (max$\delta B$) recorded is higher than 5 nT (Eq. (2.3)) are listed.

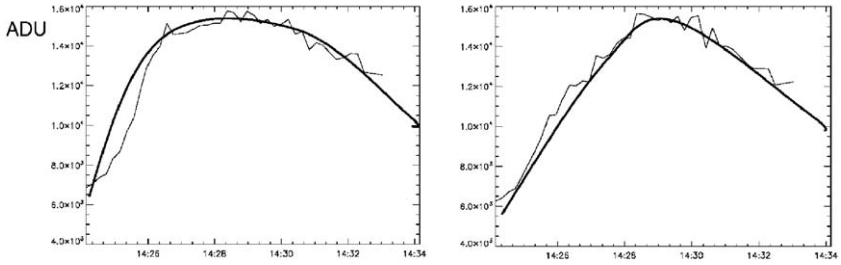


**Fig. 2.** Energy radiation at each ribbon, showing their different shapes, for the December 13, 2001 flare. The units of measurement are Analog Digital Units (ADU).

**Table 1**
GPS receivers, listed from the lower to the higher solar zenith distance, their geographic coordinates, the maximum value of $vTEC_V$, the last quiet time before the isfe is detected, and, if possible, the time when the maximum value was recorded (in minutes from 14:00 UT).

| Observatory | Solar zenith distance (deg.) | Geographic latitude (deg.) | Geographic longitude (deg.) | Max $vTEC_V$ | Last quiet time | Time of max $vTEC_V$ value |
|---|---|---|---|---|---|---|
| GOUG | 27.24 | −40.35 | −9.87 | 5.5 | 24 | 30.5/31.5 |
| CORD | 27.41 | −31.71 | −64.47 | 5.5 | 24 | 30.5/31.5 |
| SANT | 32.81 | −33.15 | −70.67 | 5.3 | 24 | 30.5/31.5 |
| RIOG | 39.26 | −53.79 | −67.75 | 5.7 | 24 | 31.5 |
| SUTH | 49.68 | −32.38 | 20.81 | 4.2 | 24 | 33.5 |
| MAS1 | 54.26 | 27.76 | −15.63 | 5 | 24 | 30.5 |
| HARO | 56.54 | −25.89 | 27.69 | 4.4 | 24 | 31.5 |
| HARB | 56.56 | −25.88 | 27.70 | 4.3 | 24 | 31.5 |
| GALA | 58.10 | 37.74 | −25.66 | 5.3 | 24 | 33.5 |
| PDEL | 61.55 | −0.74 | −90.30 | 5.3 | 24 | |
| BRMU | 62.37 | 32.37 | −64.70 | 5.5 | 24 | |
| SYOG | 62.94 | −69.00 | 39.58 | 3.1 | 24 | 30.5 |
| MADR | 69.74 | 40.43 | −4.25 | 3.2 | 25 | 32.5 |
| MAW1 | 71.58 | −67.60 | 62.87 | 2.7 | 24 | 30.5 |
| GODE | 73.47 | 39.02 | −76.83 | 5.3 | 24 | 35.5 |
| USNO | 73.51 | 38.92 | −77.06 | 5 | 24 | |
| WES2 | 73.90 | 42.61 | −71.49 | 4.4 | 25 | 34.5 |
| CAGL | 74.64 | 39.13 | 8.97 | 3.5 | 24 | 34.5 |
| MALI | 75.22 | −2.99 | 40.19 | 3.7 | 24 | |
| NOT1 | 76.31 | 36.87 | 14.99 | 2.1 | 25 | 35.5 |
| GRAS | 77.18 | 43.75 | 6.92 | 3.5 | 24 | 34.5 |
| NRC1 | 77.94 | 45.45 | −75.62 | 3.6 | 24 | 35.5 |
| ALGO | 79.40 | 45.96 | −78.07 | 4.0 | 25 | 35.5 |
| ZIMM | 79.84 | 46.87 | 7.46 | 4.0 | 25 | 35 |
| MATE | 79.87 | 40.65 | 16.70 | 2.0 | 25 | 33.5 |
| MEDI | 79.98 | 44.52 | 11.65 | 2.6 | 25 | 35.5 |
| HERS | 80.32 | 50.87 | 0.33 | 2.5 | 24 | 33 |
| NPLD | 80.57 | 51.42 | −0.34 | 2.7 | 24 | 33.5 |
| BRUS | 81.70 | 50.80 | 4.36 | 3.2 | 24.5 | |
| KERG | 81.89 | −49.35 | 70.25 | 2.0 | 24 | 31.5 |
| OBE2 | 82.46 | 48.10 | 11.30 | 3.6 | 25 | |
| ORID | 82.50 | 41.12 | 20.80 | 2.0 | 25 | 31.5 |
| SCH2 | 82.64 | 54.83 | −66.83 | 3.8 | 24 | 35.5 |
| NLIB | 83.37 | 41.77 | −91.57 | 3.5? | 24 | 32.5 |
| POTS | 86.37 | 52.38 | 13.07 | 2.2 | 25 | 33.5 |
| NICO | 87.12 | 35.14 | 33.39 | 1.8? | 25 | |
| BUCU | 87.64 | 44.46 | 26.12 | 2.0 | 25 | 33.5 |
| BOR1 | 87.90 | 52.10 | 17.07 | 2.0 | 25 | |
| UZHL | 88.11 | 48.63 | 22.30 | 2.0 | 25 | |
| HOFN | 88.79 | 64.27 | −15.20 | 2.4 | 25 | 32.5 |
| ANKR | 89.16 | 39.89 | 32.76 | 1.6 | 25 | 34.5 |

Fig. 8 shows that the increase phase of $\delta B$ is faster than the decrease phase; the $\delta B$ recorded by stations located at high latitudes – PBQ, MAW, and SBA – present oscillation due to the existence of high-latitude irregularities; a similar effect is detected with $vTEC_V$. At the mid latitude HBK, a superimposed pre-existing oscillation is recorded.

Fig. 9 shows the geographical distribution of max$\delta B$, as they were produced simultaneously all over the world; the gsfe at HUA was not represented so as not to distort the figure.

The main aspects can be summarised as follows:

- The last quiet $B$ time and max$\delta B$ are reached at 14:24 (or 14:25) UT and at 14:30 UT, respectively, and last for some 30 min, except for VSS, KOU, HUA, and MBO, whose gsfe are recorded at midday and are located close to the equator.
- VSS is the observatory closer to the SSP when the solar flare is produced.

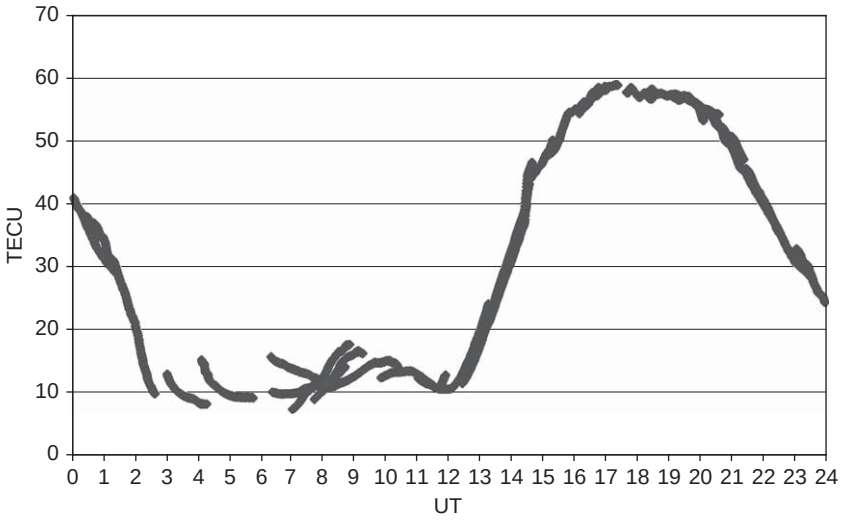


**Fig. 3.** Daily *vTEC* obtained for ALGO GPS station on December 13, 2001.

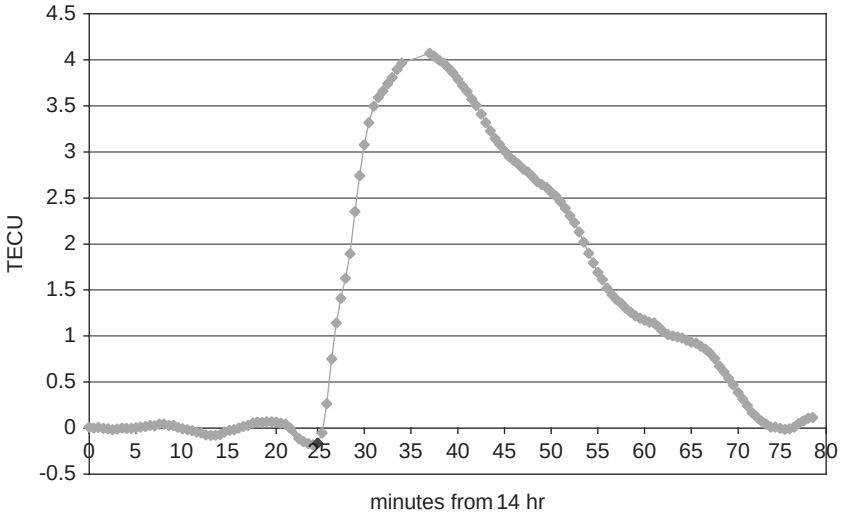


**Fig. 4.** $vTEC_V$ corresponding to data from one satellite received at ALGO station; the black point represents the quiet value considered to be the last (14:25 UT).

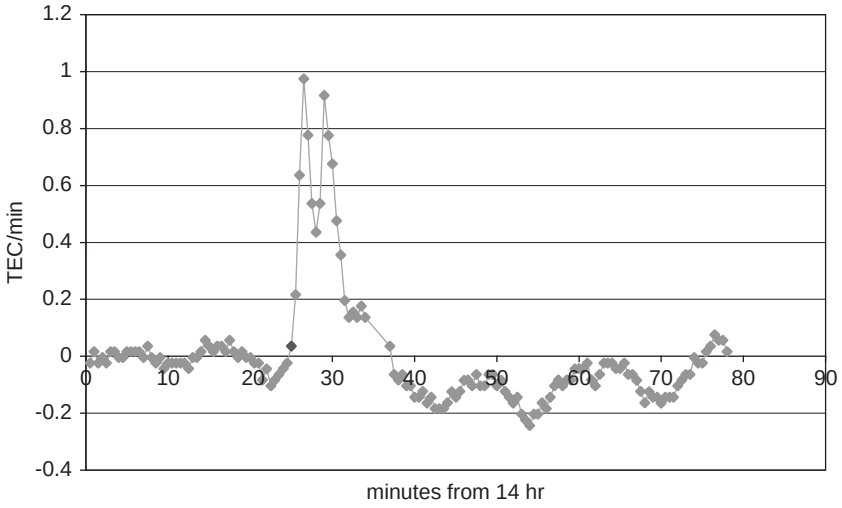


**Fig. 5.** $rvTEC_V$ obtained from data from one of the satellites at ALGO station from 14:00 UT; it shows two maxima, separated from each other by 2.5 min; the last quiet time of isfe amplitude is represented by a black point.

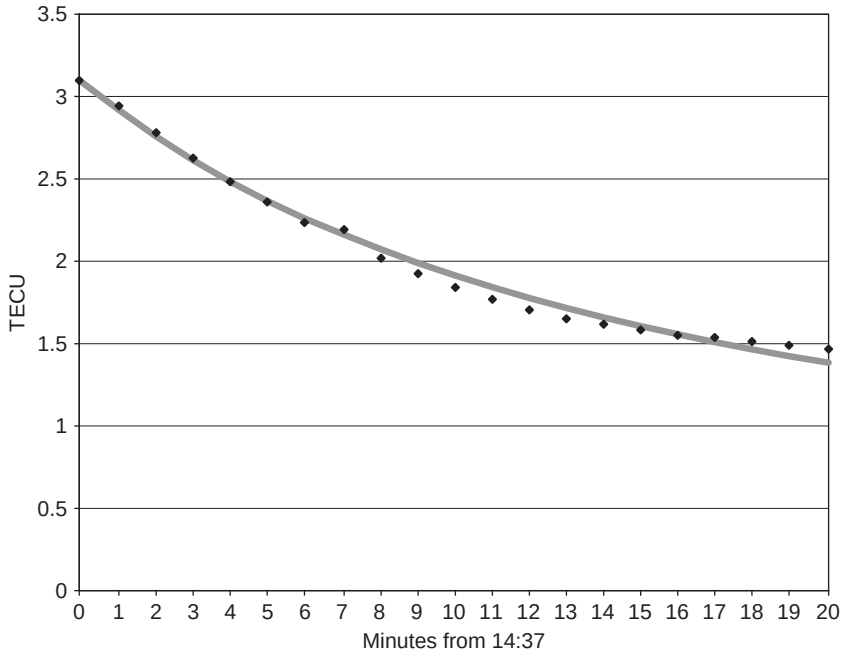


**Fig. 6.** The black points represent the $vTEC_V$ corresponding to data from one satellite received at SUTH station from 14:37; the grey curve shows the fitted $vTEC_V$ computed from Eq. (3.5) for the recovery phase of the $vTEC_V$.

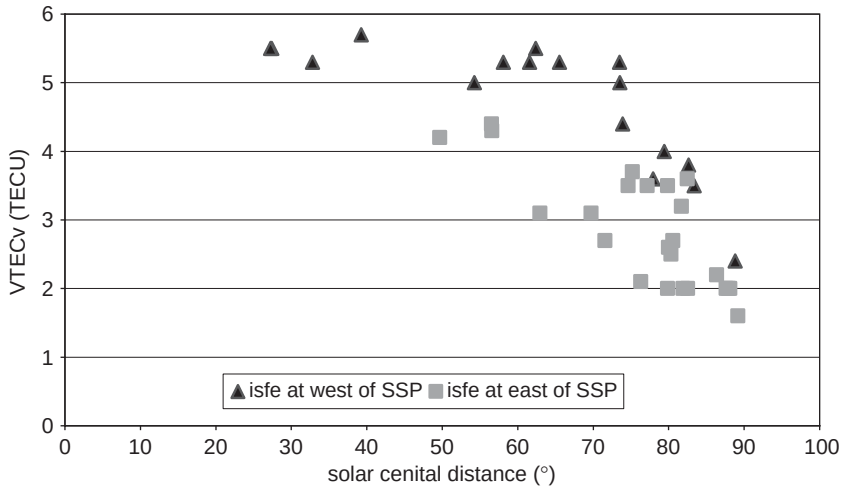


**Fig. 7.** Smoothed values of max$vTEC_V$; the data were gridded using the Kriging method and the Mollweide projection. GPS stations listed in Table 2 are superimposed as points.

- HUA, under the equatorial electrojet ($\mathrm{dip} \approx 1^\circ$, $\delta Z \approx -2$ nT), recorded the largest $\delta B$ although its distance to the SSP is not the shortest.
- AAE, close to the equatorial electrojet ($\mathrm{dip} \approx 1^\circ$, $\delta Z \approx 1$ nT), shows $\delta B$ smaller than other observatories at the same distance, possibly due to the presence of the counter-electrojet; $\delta X$(MBO) changes its sign, producing more than a maximum of $\delta B$.
- The beginning of the gsfe at observatories located to the northeast of the SSP is delayed in relation to others at the same distance.
- The gsfe is observed beyond the solar zenith angle of 90° due to ionospheric currents.
- Values for $\delta B$ derived from PBQ, CSY, and DRV, close to the auroral electrojet, are larger than those obtained from other observatories located at the same solar zenith angle.
- SJG and GUI, located near the focus (vortex) of the ionospheric currents, recorded $\delta X = 0$ nT.
- $\delta Y$, recorded by TSU observatory, changes its sign during the flare and the value is always small.
- $\delta B$ recorded by HBK displayed an oscillation and reached three maxima at 14:31, 14:34, and 14:37 UT; its $\delta X \approx 0$ and it is overflown by a meridional southward current.
- HER and LMM have $\delta X \approx 0$, which accounts for the presence of the meridional current as in HBK.
- NAQ and SBA are recorded with a pre-existing oscillation.
- The observatories located to the northwest of SSP (FRD, STJ, and OTT) recorded larger max$\delta B$ than those located to the northeast (EBR, SPT, or HAD). This result is in agreement with the max$vTEC$v geographical distribution (Fig. 6).
- The max$\delta B$ is larger in the local morning than in the local afternoon.

Table 4 lists the observatories that recorded max$\delta B \geq 17$ nT: the intensity of the two maxima (max1$(dB)'$, max2$(dB)'$) (Eq. (2.4)),

**Table 2**
$rvTEC_V$ maxima (in TECU/min); the first maximum is detected at 14:26.5 and the second at 14:29 UT.

| Observatory | 1st max $rvTEC_V$ values | 2nd max $rvTEC_V$ values |
|---|---|---|
| GOUG | 1.9 | 1.6 |
| CORD | 2.0 | 1.6 |
| SANT | 1.8 | 1.3 |
| RIOG | 1.6 | 1.2 |
| SUTH | 1.4 | 1.0 |
| MAS1 | 1.3 | 0.9 |
| HRAO | 1.4 | 1.2 |
| HARB | 1.4 | 1.0 |
| GALA | 1.0 | 0.9 |
| PDEL | 1.5 | 1.2 |
| BRMU | 1.6 | 1.4 |
| SYOG | 1.0 | 0.7 |
| MADR | 1.0 | 0.8 |
| MAW1 | 0.9 | 0.6 |
| GODE | 1.3 | 1.1 |
| USNO | 1.3 | 1.2 |
| WES2 | 1.2 | 1.1 |
| CAGL | 1.3 | 0.8 |
| MALI | 1.1 | 1.0 |
| NOT1 | 0.9 | 0.8 |
| GRAS | 1.3 | 1.2 |
| NRC1 | 0.9 | 0.8 |
| ALGO | 0.9 | 0.9 |
| ZIMM | 0.8 | 0.7 |
| MATE | 0.5 | 0.5 |
| MEDI | 0.7 | 0.5 |
| HERS | 0.6 | 0.4 |
| NPLD | 0.4 | 0.5 |
| BRUS | 0.7 | 0.6 |
| KERG | 0.6 | 0.5 |
| OBE2 | 0.5 | 0.6 |
| ORID | 0.4 | 0.4 |
| SCH2 | 0.5 | 0.5 |
| NLIB | 0.6 | 0.5 |
| POTS | 0.4 | 0.4 |
| BUCU | 0.8 | 0.8 |
| BOR1 | 0.5 | 0.45 |
| UZHL | 0.2 | 0.2 |
| HOFN | 0.2 | 0.2 |
| ANKR | 0.3 | 0.4 |

and the time when they take place. These two maxima are recorded at the same instants of the two narrow ribbons' maxima (Section 2). Generally, max1$(dB)'$ is larger than max2$(\delta B)'$ and they are separated by two or three minutes; max$\delta B$ is reached after the max2$\delta B'$; and there are a few stations (HBK, LMM) that recorded only one: max1$\delta B'$.

### 3.4. isfe and gsfe decrease

To analyse the decreasing phase of the solar flare effect, the decreases in isfe and gsfe are compared.

The solar flare flux decreases in X-rays during the interval [14:32, 14:55] UT by an exponential; assuming $A\exp(-kt)$, we obtained $A = 0.4568\,\mathrm{erg\,cm^{-2}\,s^{-1}}$ and $k = 0.156$/min (see Fig. 1).

On the other hand, the continuity equation that expresses the electron density change rate is used to compute the decay coefficient of the $vTEC_V$ variation (Chapman and Bartels, 1940)

$$\frac{dN}{dt} = kI - \alpha N^2 - div(N\vec{v}) \tag{3.1}$$

where $kI$ is the production rate by sun radiation ionisation, $\alpha N^2$ is the loss rate by recombination at about 100 km (D–E regions), and $div(n\,\vec{v})$ expresses the loss of electrons by movement.

The decay coefficient is computed from Eq. (3.1), taking into account that during the recovery phase the solar radiation ionisation component (Fig. 1 at about 14:37 UT) and the loss of electrons by movement term are neglected.

Therefore, Eq. (3.1) can be rewritten as

$$\frac{dN}{dt} = -\alpha N^2$$

or in $vTEC_v$ terms

$$\frac{dvTEC_V}{dt} = -\alpha vTEC_V^2 \tag{3.2}$$

Solving Eq. (3.2)

$$vTEC_V(t_k) = \frac{vTEC_{v0}}{1 + \alpha vTEC_{v0}(t_k - t_0)}, \tag{3.3}$$

**Table 3**
List of the observatories where the gsfe of the solar flare at 14:23 UT on December 13, 2001 is observed, and for each one, its distance to the SSP, coordinates (plus the dip latitude for HUA and AAE), the maximum amplitude calculated for the gsfe (max$\delta B$) (Eq. (2.3)), the time of the last quiet minute before the gsfe, the time of the max$\delta B$, and the time when the gsfe is supposed ended are given.

| Observations | Zenith distance (deg.) | Geographic latitude (deg.) | Geographic longitude (deg.) | máx$\delta B$ (nT) | Last quiet time (UT) | Time of max $\delta B$. (UT) | Time of the ended $\delta B$ value (UT) |
|---|---|---|---|---|---|---|---|
| VSS | 6.0 | −22.4 | −43.6 | 69.6 | 14:24 | 14:31 | 15:07 |
| KOU | 29.5 | 2.2 | −52.7 | 26.1 | 14:24 | 14:30 | 15:13 |
| TRW | 30.7 | −43.3 | −65.3 | 18.2 | 14:24 | 14:30 | 14:57 |
| HUA | 37.9 | −12.1 (1) | −75.3 | 112 | 14:24 | 14:31 | 15:11 |
| MBO | 42.4 | 14.4 (4) | −17 | 31.3 | 14:23 | 14:35 | 15:24 |
| LIV | 42.5 | −62.7 | −60.4 | 28.4 | 14:24 | 14:31 | 15:00 |
| AIA | 45.6 | −65.3 | −64.3 | 39.0 | 14:24 | 14:30 | 15:00 |
| HER | 50.0 | −34.4 | 19.2 | 21.4 | 14:25 | 14:32 | 14:57 |
| SJG | 50.3 | 18.4 | −66.1 | 18.4 | 14:24 | 14:30 | 15:00 |
| TSU | 51.0 | −19.2 | 17.7 | 8.8 | 14:24 | 14:30 | 14:51 |
| GUI | 55.2 | 28.3 | −16.4 | 21.3 | 14:24 | 14:30 | 14:55 |
| HBK | 58.5 | −25.9 | 27.7 | 17.7 | 14:25 | 14:31 | 14:57 |
| BNG | 60.9 | 4.3 | 18.6 | 18.9 | 14:24 | 14:31 | 14:50 |
| TAM | 61.9 | 22.8 | 5.5 | 11.4 | 14:25 | 14:32 | 14:57 |
| LMM | 62.7 | −25.9 | 32.6 | 25.9 | 14:24 | 14:30 | 14:52 |
| SPT | 69.9 | 39.6 | −4.3 | 19.9 | 14:24 | 14:31 | 15:18 |
| FRD | 72.1 | 38.2 | −77.4 | 30.3 | 14:24 | 14:30 | 14:55 |
| STJ | 72.1 | 47.6 | −52.7 | 36.3 | 14:24 | 14:31 | 14:57 |
| MAW | 72.4 | −67.6 | 62.9 | 34.4 | 14:25 | 14:32 | 14:56 |
| CZT | 72.8 | −46.4 | 51.9 | 8.7 | 14:25 | 14:30 | 14:50 |
| EBR | 72.9 | 40.8 | 0.5 | 20.6 | 14:25 | 14:30 | 14:55 |
| BSL | 73.5 | 30.4 | −89.6 | 22.9 | 14:24 | 14:30 | 14:55 |
| OTT | 76.9 | 45.4 | −75.5 | 34.1 | 14:24 | 14:30 | 14:57 |

Table 3 (*continued*)

| Observations | Zenith distance (deg.) | Geographic latitude (deg.) | Geographic longitude (deg.) | máx$\delta B$ (nT) | Last quiet time (UT) | Time of max $\delta B$. (UT) | Time of the ended $\delta B$ value (UT) |
|---|---|---|---|---|---|---|---|
| SBA | 78 | −77.8 | 166.8 | 24.9 | 14:25 | 14:29 | 14:53 |
| CLF | 79.5 | 48 | 2.3 | 17.6 | 14:25 | 14:30 | 14:52 |
| HAD | 79.6 | 51 | −4.5 | 21.7 | 14:25 | 14:30 | 14:57 |
| DLR | 80.8 | 29.5 | −100.9 | 15.7 | 14:25 | 14:31 | 14:55 |
| AAE | 80.9 | 9.0 (1) | 38.8 | 6.2 | 14:27 | 14:32 | 14:57 |
| DOU | 82.1 | 50.1 | 4.6 | 15.6 | 14:25 | 14:30 | 14:57 |
| MAB | 82.7 | 50.3 | 5.7 | 12.4 | 14:26 | 14:30 | 14:50 |
| FUR | 83.5 | 48.2 | 11.3 | 9.2 | 14:25 | 14:31 | 14:50 |
| ESK | 83.7 | 55.3 | −3.2 | 15.3 | 14:25 | 14:31 | 14:52 |
| NAQ | 84.6 | 61.2 | −45.4 | 13.3 | 14:25 | 14:29 | 14:55 |
| BDV | 85.1 | 49.1 | 14 | 7.8 | 14:26 | 14:30 | 14:50 |
| NCK | 85.7 | 47.6 | 16.7 | 6.6 | 14:26 | 14:30 | 14:47 |
| PBQ | 85.7 | 55.3 | −77.7 | 17 | 14:25 | 14:32 | 14:55 |
| THY | 85.9 | 46.9 | 17.9 | 6.3 | 14:26 | 14:30 | 14:50 |
| HRB | 86.7 | 47.9 | 18.2 | 5.8 | 14:26 | 14:31 | 14:57 |
| WNG | 86.7 | 53.8 | 9.1 | 6.8 | 14:25 | 14:31 | 14:50 |
| NGK | 86.9 | 52.1 | 12.7 | 7.3 | 14:26 | 14:30 | 14:50 |
| CSY | 87.2 | −66.3 | 110.5 | 19.3 | 14:25 | 14:31 | 115:01 |
| LER | 88.3 | 60.1 | −1.2 | 6.5 | 14:26 | 14:33 | 14:50 |
| BOU | 89.5 | 40.1 | −105.2 | 10 | 14:25 | 14:33 | 14:55 |
| TUC | 89.5 | 32.3 | −110.8 | 5.2 | 14:25 | 14:30 | 14:54 |
| DRV | 90.1 | −66.7 | 140 | 19.3 | 14:25 | 14:30 | 14:52 |
| FRN | 98.2 | 37.1 | −119.7 | 6.4 | 14:25 | 14:31 | 14:55 |
| NEW | 100.8 | 48.3 | −117.1 | 6.0 | 14:25 | 14:33 | 14:57 |
| VIC | 104.8 | 48.5 | −123.4 | 5.4 | 14:24 | 14:33 | 14:55 |

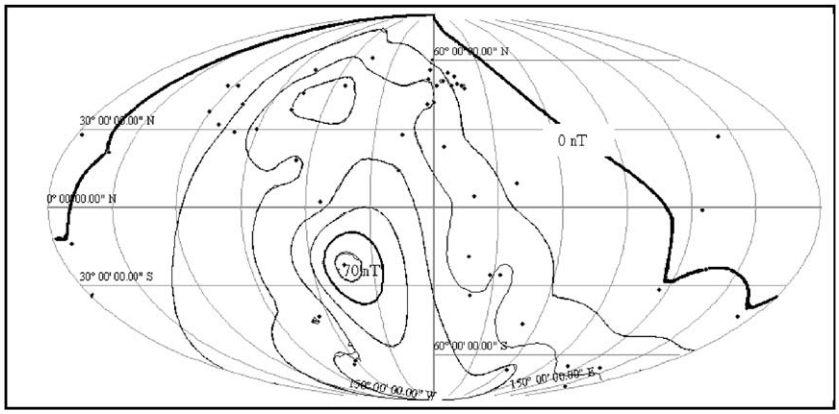


**Fig. 8.** Calculated $\delta B$ for some of the observatories from Table 3 recorded for each minute on December 13, 2001, during a solar flare.

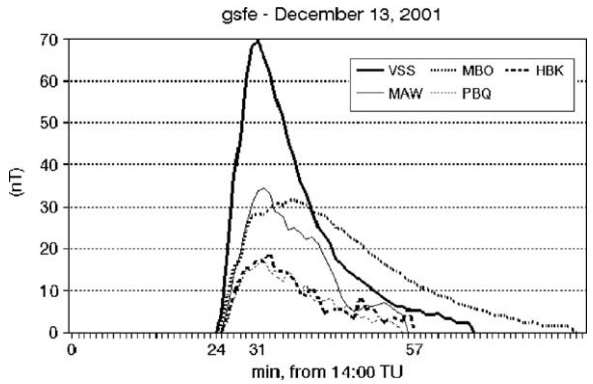


**Fig. 9.** Max$\delta B$ for each observatory from Table 3, smoothed after the Kriging method and the Mollweide projection, as if they were recorded simultaneously all over the world; dots indicate the positions of the geomagnetic observatories whose data are used here; HUA máx$\delta B$ is not represented here to avoid distorting the figure; and to complete the data $\delta B = 0$ has been added for ASP (−23.8, 133.9), CBI (27.1°, 142.2°), API (−13.8°, 188.2°), GNA (−31.8°, 115.9°), HON (21.3°, 202°), EYR (−43.3°, 172.4°), TND (−1.3°, 124.9°), and MID (28.2°, 182.6°).

where $t_0$ is the time of the beginning of the recovery phase and $\alpha$ the decay coefficient. Using the least squares method, the values of $vTEC_{V0}$ and $\alpha$ are estimated. Fig. 10 shows an example using SUTH GPS station data.

On the other hand, the decrease in $\delta B$ can be fitted by an exponential by least squares, the expression

$$(\delta B)' = -k \cdot \delta B;$$

$k$ (1/min) represents the decrease in the gsfe; it is calculated from 14:36 UT, when the X-ray intensity has decreased about $e^{-1}$; thus, from the difference equation (Box and Jenkins, 1976)

$$\delta B_i - \delta B_{i-1} = -k.\delta B_i;$$

and with the condition

$$\frac{\partial}{\partial k}\sum(\delta B_i - \delta B_{i-1}/(1+k))^2 = 0 \Rightarrow k = \frac{\sum \delta B_{i-1}^2}{\sum \delta B_i \cdot \delta B_{i-1}} - 1 \qquad (3.4)$$

the calculation of the successive values $\delta B_{ic}$ is

$$\delta B_{ic} = \delta B_{(i-1)c}/(1+k) \qquad (3.5)$$

and the standard deviation $\sigma^2$ is

$$\sigma^2 = \frac{\sum(\delta B_{ic} - \delta B_i)^2}{n} \tag{3.6}$$

with $n$ being the number of data.

Table 4 shows the $k$ and $\sigma^2$ values for geomagnetic observatories that recorded max$\delta B > 17$ nT.

Fig. 11 shows the decrease phase of gsfe recorded by observatory OTT.

To compare the decrease phases of isfe and gsfe, the data from magnetic observatories and GPS receivers which are separated by less than 5° are used.

Table 5 shows the decay coefficients of $\delta B$, $k$, and $vVTEC_V$, $\alpha$, and values for the last quiet time and the time of maximum variations.

From the previous analysis at 14:56, the solar X-ray has decayed by about 96% and $\Delta b$ is between 80% and 95% while at the same time $vTEC_V$ has decayed by only 35–50%.

**Table 4**
Observatories with max$\delta B \geq 17$ nT where the two bigger rises of $\delta B$ (Eq. (2.4)) are shown and the instants they are produced; in most cases $(\delta B)'$ (in nT/min) has two maxima; also shown are the constant decay ($k$, in 1/min) and the standard deviation ($\sigma^2$) calculated from 14:36 UT; for MBO, $k$ and $\sigma^2$ are calculated from 14:43 UT because its gsfe had not reached the maximum at 14:36 UT (see Table 1).

| Observations | max1$(dB)'$ | Time | max2$(dB)'$ | Time | $k$ | $\sum^2$ |
|---|---|---|---|---|---|---|
| VSS | 17.7 | 14:27 | 13.7 | 14:29 | 0.119 | 0.41 |
| KOU | 7.4 | 14:26 | 6.4 | 14:29 | 0.058 | 0.64 |
| TRW | 4.4 | 14:27 | 4.4 | 14:29 | 0.106 | 0.70 |
| HUA | 28.0 | 14:26 | 19.5 | 14:29 | 0.095 | 4.09 |
| MBO | 6.7 | 14:26 | 7.0 | 14:29 | 0.059 | 1.4 |
| LIV | 7.1 | 14:27 | 6.1 | 14:28 | 0.071 | 2.84 |
| AIA | 13.4 | 14:26 | 7.2 | 14:28 | 0.141 | 0.75 |
| HER | 5.0 | 14:27 | 4.6 | 14:29 | 0.110 | 0.40 |
| SJG | 4.3 | 14:27 | 3.4 | 14:29 | 0.095 | 0.11 |
| GUI | 5.2 | 14:27 | 5.4 | 14:29 | 0.119 | 0.43 |
| HBK | 5.0 | 14:27 | | | 0.134 | 5.33 |
| BNG | 4.1 | 14:26 | 3.8 | 14:29 | 0.163 | 0.24 |
| LMM | 6.5 | 14:26 | | | 0.148 | 0.08 |
| SPT | 5.0 | 14:27 | 4.1 | 14:29 | 0.073 | 0.30 |
| FRD | 8.5 | 14:27 | 6.6 | 14:29 | 0.160 | 0.28 |
| STJ | 10.3 | 14:27 | 7 | 14:29 | 0.159 | 0.29 |
| MAW | 7.2 | 14:27 | | | 0.089 | 7.36 |
| EBR | 6.2 | 14:27 | 4 | 14:29 | 0.136 | 0.36 |
| OTT | 9.4 | 14:27 | 5.8 | 14:29 | 0.129 | 0.78 |
| SBA | 8.3 | 14:27 | 5.9 | 14:29 | 0.077 | 2.01 |
| CLF | 6.6 | 14:27 | 3.5 | 14:29 | 0.199 | 0.32 |
| HAD | 7.9 | 14:27 | 4.9 | 14:29 | 0.155 | 0.21 |
| PBQ | 5.8 | 14:27 | 1.1 | 14:31 | 0.092 | 2.13 |
| CSY | 5.1 | 14:27 | 5.0 | 14:29 | 0.095 | 0.97 |

## 4. Discussion

Some general characteristics can be summarised as follows:

- The beginning of the solar flare (14:24 UT) is previous to the isfe or the gsfe.
- The maximum $\delta B$ is always reached simultaneously with or later than the maximum X-ray intensity.
- The maximum $vTEC_V$ is recorded later than max$\delta B$ and maximum X-ray intensity.
- The observatories located northwest of the SSP recorded larger $vTEC_V$ and $\delta B$ than those located to the northeast.
- $(\delta B)'$ and $rvTEC_V$ generally present two maxima.
- Max$\delta B$ depends on the solar zenith angle and the intensity and location of currents. Observatories located close to the electrojets recorded $\delta B$ larger than those obtained by observatories at the same solar zenith angle. The increase in the electrical conductivity could produce the large enhancement of gsfe near the equatorial electrojet as proposed by Nagata (1952).
- Max$vTEC_V$ depends on the solar zenith angle and the processes of production and loss of electrons at the time when the flare arrives. The enhancement of $vTEC$ is larger in the local morning than in the local afternoon. Our results are similar to those obtained by Zhang and Xiao (2000), but they are very different from those obtained by Matsoukas et al. (1972) and Zhang et al. (2002).
- The isfe decrease phase always starts after it is recorded by gsfe and sfe, possibly due to a still growing ionisation in the upper ionosphere.

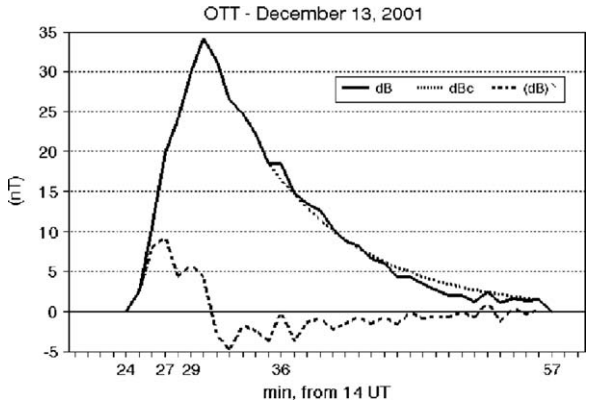


**Fig. 11.** $\delta B$ variation (in nT) from OTT and fitted $\delta Bc$ after Eq. (3.4) ($k$ in Table 4); variation $(\delta B)'$ (in nT/min) with the two maxima.

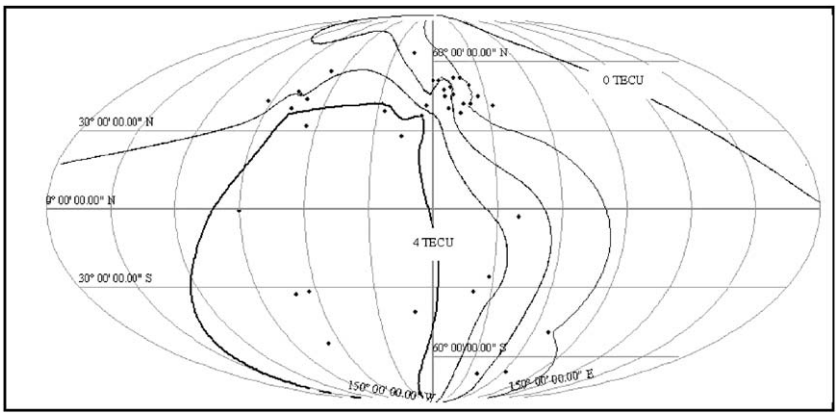


**Fig. 10.** Maximum $vTEC_V$ in relation to distance to the solar zenith distance, after Table 1.

**Table 5**
The decay coefficients of $\delta B$, $k$, and $vVTEC_V$, $\alpha$, and values of the last quiet time and time of maximum variations.

| Magnetic observations | GPS receiver | $k$ (1/min) $\alpha$ | $T$(min) | Last quiet time (UT) | Time of max variation (UT) |
|---|---|---|---|---|---|
| TRW (dist = 30.7°) | GOUG | 0.106<br>0.054 | 9 | 14:24<br>14:24 | 14:30<br>14:31 |
| HER (dist = 50.0°) | SUTH | 0.110<br>0.020 | 9 | 14:25<br>14:24 | 14:32<br>14:33 |
| GUI (dist = 55.2°) | MAS1 | 0.119<br>0.039 | 8 | 14:24<br>14:24 | 14:30<br>14:30.5 |
| FRD (dist = 72.1°) | USNO | 0.160<br>0.018 | 6 | 14:24<br>14:24 | 14:30 |
| OTT (dist = 76.9°) | ALGO | 0.129<br>0.019 | 8 | 14:24<br>14:25 | 14:30<br>14:35.5 |
| CLF (dist = 79.5°) | ZIMM | 0.199<br>0.007 | 5 | 14:25<br>14:25 | 14:30<br>14:35 |

They are computed from the observations of nearby GPS stations and geomagnetic observatories.

- The decay constant $k$ for gsfe and the solar flare X-ray intensity are very similar, but the isfe decays more slowly due to a slower recombination rate in the upper atmosphere than in the lower one.

## 5. Conclusions

For the solar flare X6.2 located at N16 E09 and detected by GOES from 14:24 UT, we conclude that:

- The distance between the subsolar point and each observatory is not the only parameter to be considered; for gsfe the intensity and position of the currents overflying them (as can be seen with the electrojets) should also be considered, whereas isfe (expressed by $vTEC_V$) is related to the growing and decreasing phase of the electron content not only in the lower ionosphere but also in the upper one.
- The isfes detected to the northwest of the SSP are larger than those seen to the northeast; the same occurs for the gsfe; there is a lack of data for the Southern Hemisphere and a similar comparison cannot be made.
- The gsfe (expressed by $\delta B$) and the isfe confirm known theory on the solar flare effect, and the analysis reveals that the larger $\hat{\imath}TEC_V$ to the northwest of the SSP is the cause of the enhanced $\delta B$ in this region.
- The isfe behaviour shows two stronger intensifications at the time of the Hα maxima and the same occurs for the gsfe, although the GOES X-ray does not record two maximum values. An explanation could be that radiation with wavelengths longer than those of X-rays produced the ionisation of the lower ionosphere.
- The maximum $\delta B$ is always simultaneous to or scarcely later than the maximum intensity of the X-ray and the maximum $vTEC_V$ is generally later than both of them.

## Acknowledgements

The authors are very grateful to world data centres for the free availability of the data: WDC-C Kyoto University, Japan; Service International des Indices Geomagnetiques, Bureau des Publications SIIG, France; Consejo Nacional de Investigaciones Científicas y Técnicas, Argentina; Facultad de Ciencias Exactas y Naturales (Universidad de Buenos Aires), Argentina; and Facultad de Ciencias Astronómicas y Geofísicas (Universidad Nacional de La Plata), Argentina.

## References

Aarons, J., Mendillo, M., Yantosca, R., 1997. GPS phase fluctuations in the equatorial region during sunspot minimum. Radio Science 32 (4), 1535–1550.
Afraimovich, E.L., Altynsev, A.T., Kosogorov, E.A., 2001. Ionospheric effects of the solar flares of 23 September 1998 and 29 July 1999 as deduced from global GPS network data. Journal of Atmospheric and Solar-Terrestrial Physics 63, 1841–1849.
Afraimovich, E.L., Altynsev, A.T., Grechnev, V.V., Leonovich, L., 2002. The response of the ionosphere to faint and bright solar flares as deduced from global GPS network data. Annals of Geophysics 45 (1), 31–40.
Afraimovich, E.L., Altyntsev, A.T., Kosogorov, E.A., Larina, N.S., Leonovich, L.A., 2000. Ionospheric effects of the solar flares of September 23, 1998 and July 29, 1999 as deduced from global GPS network data. Journal of Atmospheric and Solar-Terrestrial Physics 63 (17), 1841–1849.
Baker, W.G., Martyn, D.F., 1953. Electric currents in the ionosphere: the conductivity. Philosophical Transactions of the Royal Society (London) A246, 281–294.
Box, G.E.P., Jenkins, G.M., 1976. Time series analysis, forecasting and control. Holden-Day series, USA.
Chapman, S., Bartels, J., 1940. Geomagnetism, Vol. 2. Oxford Press, London.
Ciraolo, L., Azpilicueta, F., Brunini, C., Meza, A., Radicella, S.M., 2007. Calibration errors on experimental slant total electron content determined with GPS. Joun. Geod. (Journal of Geodesy), Published by Springer, Berlin, doi:10.1007/s00190-006-0093-1, 111–120.
Curto, J.J., Amory-Mazaudier, C., Torta, J.M., Menvielle, M., 1994. Solar flare effecs at Ebre: regular and reversed solar flare effects, statistical analysis (1953–1985), a global case study and a model of elliptical ionospheric currents. Journal of Geophysical Research 99 (A3), 3945–3954.
Davies, K., 1980. Ionospheric Radio. Peter Peregrinus, London, p. 580.
Donnelly, R.F., 1976. The solar flare radiations responsible for sudden frequency deviations. Journal of Geophysical Research 72, 5247–5256.
García Rigo, A., Hernandez-Pajares, M., Juan, J.M., Sanz, J., 2007. Solar Flare system base don global positioning system data: first result. Advance in Space Research 39, 889–895.
Ho, C.M., Mannucci, A.J., Sparks, L., Pi, X., Lindqwister, U.V., Wilson, B.D., Iijima, B.A., Reyes, M.J., 1998. Ionospheric total electron content perturbations monitored by the GPS global network during two northern hemisphere winter storms. Journal of Geophysical Research 103 (A11), 26409–26420.
Jakowski, N., Schlüter, S., Sardon, E., 1999. Total electron content of the ionosphere during the geomagnetic storm of 10 January 1997. Journal of Atmospheric and Solar-Terrestrial Physics 61, 299–307.
Liu, J.Y., Tsai, J.H.F., Liou, Y.A., 2004. Ionospheric solar flare effects monitored by the ground based GPS receivers: theory and observations. Journal of Geophysical Research 109 (A01307).
Liu, J.Y., Lin, C.H., Chen, Y.I., Lin, Y.C., Fang, T.W., Chen, C.H., Chen, Y.C., Hwang, J.J., 2006. Solar flare signatures of the ionospheric GPS total electron content. Journal of Geophysical Research 111 (A5).
Lui, J.Y., Chiu, C.S., Lin, C.H., 1996. The solar flare radiation responsible for sudden frequency deviation and geomagnetic fluctuation. Journal of Geophysical Research 101 (A5), 10855–10862.
Matsoukas, D.A., Papagiannis, M.D., Aarons, J., et al., 1972. Correlation of solar radio bursts and sudden increases of the total electron content (SITEC) of the ionosphere. Journal of Atmospheric and Terrestrial Physics 34, 1275–1283.
Mendillo, M., 1974. Incoherent scatter observations of the ionosphere with respect to a large solar flare. Radio Science 9, 197–210.
Mendillo, M., Klobuchar, J.A., Fritz, R.B., da Rosa, A.V., Kersley, L., Yeh, K.C., Flaherty, B.J., Rangaswamy, S., Schmid, P.E., Evans, J.V., Schodel, J.P., Matsoukas, D.A., Koster, J.R., Webster, A.R., Chin, P., 1974. Behavior of the ionospheric Fregion during the great solar flare of August 7, 1972. Journal of Geophysical Research 79, 665–672.

Meza, A., Van Zele, M.A., Brunini, C., Cabassi, R., 2005. Vertical total electron content at subauroral and mid-south latitude, during geomagnetic storms. Journal of Atmospheric and Solar terrestrial Physics (JASTP) (67), 4315–4323.

Nagata, T., 1952. Characteristics of the solar flare effects (Sqa) on geomagnetic field at Huancayo (Perú) and at Kakioka (Japan). Journal of Geophysical Research 57, 1–14.in: The equatorial electrojet: Magnetic and Ionospheric Effects, by R.G. Rastogi, at Geomagnetism, Vol. 3, Jacobs, J.A. (Ed.), Academic Press.

Rastogi, R.G., Kaushika, N.D., Trivedi, N.B., 1965. Solar flare crochet and sudden commencement in H within the equatorial electrojet region. Journal of Atmosphere and Terrestrial Physics 27, 663–668.in: The equatorial electrojet: Magnetic and Ionospheric Effects, by R.G. Rastogi, at Geomagnetism, Vol. 3, Jacobs, J.A. (Ed.), Academic Press.

Rastogi, R.G., 1998. Storm sudden commencements in geomagnetic H, Y and Z fields at the Equatorial Electrojet Station, Annamalainagar. Journal of Atmospheric and Solar-Terrestrial Physics 60, 1295–1302.

Sardon, E., Rius, A., Zarraoa, N., 1994. Estimation of the transmitter and receiver differential biases and the ionospheric total electron content from Global Positioning System observations. Radio Science 29, 577–586.

Thome, G.D., Wagner, L.S., 1971. Electron density enhancements in the E and F regions of the ionosphere during solar fares. Journal of Geophysical Research 76, 6883–6895.

Van Sabben, D., 1961. Ionospheric current systems of ten IGY-solar flare effects. Journal of Atmospheric and Terrestrial Physics 22, 32–42.

Volland, H., Taubenheim, J., 1958. On the ionospheric current system of the geomagnetic solar flare effect (s.f.e.). Journal of Atmospheric and Terrestrial Physics 12, 258–265.

Wan, W., Liu, L., Yuan, L.H., Ning, B., Zhang, S., 2005. The GPS measured SITEC caused by the very intense solar flare on July 14, 2000. Advances in Space Research 36 (12), 2065–2069.

Zhang, D.H., Xiao, Z., 2003. Study of the ionospheric total electron content response to the great flare on 15 April 2001 using the International GPS Service network for the whole sunlit hemisphere. Journal of Geophysical Research 1008 (A8).

Zhang, D.H., Xiao, Z., 2000. Study of the ionospheric TEC using GPS during the large solar flare burst on November 6, 1997. Chinese Science Bulletin 45, 1749–1752.

Zhang, D.H., Xiao, Z., 2005. Study of the ionospheric response to the 4B flare on 28 October 2003 using International GPS Service network data. Journal of Geophysical Research 110 (A03307).

Zhang, D.H., Xiao, Z., Igarashi, K., Ma, G.Y., 2002. GPS-derived ionospheric total electron content response to a solar flare that occurred on 14 July 2000. Radio Science 37 (5).